Sensing Global Changes in the Local Patterns of Energy Consumption in Cities During the Early Stages of the COVID-19 Pandemic

Francisco Rowe (F.Rowe-Gonzalez@liverpool.ac.uk)
Geographic Data Science Lab, Department of Geography and Planning, University of Liverpool
https://orcid.org/0000-0003-4137-0246
Caitlin Robinson
Geographic Data Science Lab, Department of Geography and Planning, University of Liverpool
Nikos Patias
Geographic Data Science Lab, Department of Geography and Planning, University of Liverpool

Research Article

Keywords: COVID-19, energy consumption, mobility, night-time light satellite imagery, cities

Posted Date: August 26th, 2021

DOI: https://doi.org/10.21203/rs.3.rs-846222/v1

Sensing Global Changes in the Local Patterns of Energy Consumption in Cities During the Early Stages of the COVID-19 Pandemic

Francisco Rowe[1,*], Caitlin Robinson[1], and Nikos Patias[1]

[1]Geographic Data Science Lab, Department of Geography and Planning, University of Liverpool, Liverpool, United Kingdom
[*]F.Rowe-Gonzalez@liverpool.ac.uk

ABSTRACT

COVID-19, and the wider social and economic impacts that a global pandemic entails, have led to unprecedented reductions in energy consumption globally. Whilst estimates of changes in energy consumption have emerged at the national scale, detailed sub-regional estimates to allow for global comparisons are less developed. Using night-time light satellite imagery from December 2019–June 2020 across 50 of the world's largest urban conurbations, we provide high resolution estimates ($450m^2$) of spatio-temporal changes in urban energy consumption in response to COVID-19. Contextualising this imagery with modelling based on indicators of mobility, stringency of government response, and COVID-19 rates, we provide novel insights into the potential drivers of changes in urban energy consumption during a global pandemic. Our results highlight the diversity of changes in energy consumption between and within cities in response to COVID-19, somewhat refuting dominant narratives of a shift in energy demand away from dense urban areas. Further modelling highlights how the stringency of the government's response to COVID-19 is likely a defining factor in shaping resultant reductions in urban energy consumption.

Introduction

COVID-19, and the wider social and economic impacts that a global pandemic entails, have substantially reconfigured energy consumption patterns[1], causing the biggest fall in global energy investment in history[2]. With GDP shrinking by -3.3% globally during 2020 and recoveries diverging[3], energy demand fell by -4% during 2020 compared to 2019 levels, impacting advanced economics most severely[4]. Global CO2 emissions also fell by -5.8% during 2020 relative to 2019[2]. Kanda and Kivimaa[5] characterise COVID-19 as a 'landscape shock' during which rapid political action and emergency legislation - what energy transitions literature terms 'disruptive policies'[6] - have shaped the trajectory of energy transitions in unprecedented ways. Where previously government efforts to operationalise low carbon policies have been critiqued as slow and ineffectual, responses to COVID-19 have been characterised by suddenness and scale. Arguably cities have been central to these shifts[7,8]. However, there is evidence that many changes are temporary as CO2 emissions have returned to pre-pandemic levels during 2021[9].

Like many aspects of the pandemic, energy consumption changes are socially, spatially and temporally uneven[10–13]. During the early stages of the pandemic new energy consumption practices emerged as societies locked down to differing extents, energy-intensive industries were suspended and people spent a greater proportion of time at home. These patterns are especially stark in cities where energy and associated infrastructures are an integral part of life. In many contexts evidence has emerged of a subsequent shift in consumption from commercial, industrial and transportation energy sectors into the domestic sphere[14]. Coupled with accelerated drops in energy prices[15], these reconfigurations have tested the finances and flexibility of electricity grids[5] and exacerbated existing energy-related inequalities[16–19].

To better understand the impact of COVID-19 on energy consumption, national-scale evidence has emerged[1,4,20,21]. However, changes in energy consumption are likely to be highly locally specific, varying according to socio-economic and urban structure, geographic context, and institutional or cultural change stimulated by COVID-19[5]. Subsequently, Acuto et al.[22] make the case for "seeing COVID-19 like a city" recognising the need to reach "beyond the confines of state-centric views to embrace the political-economic complexity of the 'urban'" (p.978). In the absence of detailed administrative energy-related statistics, night-time light (NTL) satellite imagery can provide timely evidence of sub-regional changes in energy consumption during the pandemic[12,23].

Using an urban lens, we analyse the early stages of the pandemic when COVID-19 spread rapidly via (inter)national linkages between major global cities, allowing us to evaluate changes in urban energy consumption as the pandemic first unfolded. We analyse NTL imagery from three months before and after 11th March 2020 (i.e. December 2019–June 2020), the date on which

the World Health Organisation (WHO) declared COVID-19 a global pandemic. Our results provide high-resolution estimates of spatiotemporal changes in urban energy consumption in response to COVID-19. To offer novel insights into potential drivers of changes in NTL intensity, we contextualise imagery with a range of sub-regional indicators of population density, COVID-19 cases and deaths, mobility estimates, and government response indicators. In doing so, the paper evidences:

1. city-scale changes in energy consumption in response to COVID-19 (Section 3);
2. shifting spatial patterns of intra-urban energy consumption (Section 4);
3. potential explanations for changes in urban energy consumption (Section 5).

Using NTL satellite imagery to analyse urban energy consumption

Patterns of energy consumption change in 50 of the largest global cities are analysed. With the exception of Milan (Italy) (included as an epicentre of the initial COVID-19 outbreak), all cities rank within the top 110 largest urban agglomerations based on population size, with over 4.2 million inhabitants as of 2020[24], and a diversity of national contexts are represented. City extent is defined using Functional Urban Area (FUA) boundaries[25] which provide a consistent classification based on density and commuting flows.

To understand changes in energy consumption in response to COVID-19 in each city, we analyse NTL satellite imagery, a well-established proxy for urban energy consumption[26]. In response to COVID-19, NTL imagery has been used to understand the initial impact on the US electricity sector[1], changes in CO2 emissions nationally[9], and changes in economic activity in the core of global megacities[27].

We use and process a monthly series of satellite images recording NTL intensity measured in radiance units ($nWcm^{-2}sr^{-1}$), to produce monthly global composites (see Methods) for between December 2019 and June 2020 (Figure 1). Each pixel within the image represents an area of $450m^2$. In analysing change in NTL intensity, it is necessary to assume that this change is the result of COVID-19 and associated restrictions, however, we acknowledge that other factors could contribute (e.g. national holidays, blackouts). Subsequently, we further contextualise the imagery with additional indicator data sets: daily national estimates of stringency of government response[28]; population density estimates[29]; confirmed COVID-19 cases[30]; and daily sub-regional mobility estimates[31].

City-scale changes in energy consumption patterns during COVID-19

Comparison of imagery from December 2019 and each month between January 2020 and June 2020 yields three city-scale summary indicators of average NTL intensity (see Methods and Supplementary Materials (SM) Table 1), each a proxy for changes in urban energy consumption (Figure 2). Firstly, the mean number of pixels indicator (left) indicates the proportion of pixels in each city for which the average change was either negative, neutral or positive. To account for variation in city size (with indicators based on number of pixels likely prioritising larger, less dense urban conurbations), a second indicator is provided based on the mean percentage of pixels (centre). Thirdly, an indicator of median percentage change illustrates the strength of change in NTL intensity (positive or negative).

Based on the mean percentage of pixels, in selected cities a high proportion of pixels experienced no change in NTL intensity during the six month period. In four cities this represented over half of pixels: Manila (53%) Osaka (60%), Melbourne (69%) and Dhaka (74%). Elsewhere, the mean percentage of pixels was overwhelmingly negative: Shanghai (56%), Beijing (51%); Johannesburg (54%), Luanda (53%), and Milan (54%). For several cities, particularly in the Middle East, change was largely positive, including Tehran (50%), Moscow (55%) and Baghdad (64%). The strength of change also varies considerably, as reflected by the median percentage change indicator. In Lima there was a large difference between the median negative (-25%) and positive percentage change (+ 22.75%) indicating considerable diversity in NTL intensity across space and time.

For other cities, the distribution of change in pixels is relatively similar for each time period (e.g. Melbourne; Osaka; Manila) (Figure 3) suggesting that the spatial distribution of NTL intensity is relatively stable over time. In Melbourne little change was experienced over time, likely reflective of stringent border closures that have enabled a national zero-COVID strategy[32]. In other cities, where there was greater variation in the distribution of change (e.g. Karachi, Tehran, Kinshasa, Mumbai) detailed examination of the intra-urban distribution of NTL intensity is useful.

Shifting spatial patterns of intra-urban energy consumption during COVID-19

Examination of the relationship between population density and NTL intensity (Figure 4) provides insight into the intra-urban distribution of energy consumption in response to COVID-19. Much attention has been paid to the risk of infection in dense urban centres[27,33], particularly during the early stages of the outbreak. This is evident in cities in which NTL intensity declined

in densely populated areas (e.g. Johannesburg; Karachi; Kinshasa; Tokyo; Toronto). However, for the majority of cities we observe little association between the variables, with some cities experiencing a relative increase in light intensity in densely populated areas (e.g. Delhi, Melbourne; Rio de Janeiro; New York).

From closer inspection of mapped NTL intensity (for imagery for all 50 cities see SM Figure 2), three distinctive spatial configurations in energy use are identified: (i) Whole city; (ii) Fragmented; and (iii) Spatially concentrated (Figure 5). This classification is not exhaustive, rather it illustrates the type, consistency and diversity of change in cities globally in response to COVID-19.

Firstly, selected cities experience a whole city change in NTL intensity. In Beijing, where a national lockdown was implemented in February, dimming of the majority of the pixels occurred (see also Addis Ababa; Beijing; Buenos Aires; Cairo; Luanda; Mexico City; Rio de Janeiro; São Paulo; Santiago; Shanghai; Toronto; Wuhan). Comparatively, in a small number of cities including Dar es Salaam, the majority of pixels brightened (see also Abidjan; Baghdad and Kabul).

Secondly, selected cities experienced fragmented changes with pixels increasing and decreasing across the city with limited spatial patterning. This was the case in Los Angeles and Singapore when lockdown restrictions were introduced in March (see also Istanbul; Johannesburg; Kuala Lumpur; London; Melbourne; Milan; New York; Osaka; Rome; Singapore; Tokyo).

Thirdly, spatially concentrated changes in NTL intensity also occurred. Spatially concentrated changes were wide-ranging, reflecting diverse urban structures. Changes in some cities were shaped by networked infrastructures illustrative of connectivity (i.e. based on roads and economic corridors) that arguably play an integral role in the spread of COVID-19[33]. In Delhi, networked infrastructures dimmed in March in response to restrictions (see also Bangkok and Lahore), whilst in Moscow infrastructures brightened. Elsewhere, change replicated classic core-versus-periphery structures of cities (Dhaka; Karachi; Lagos; Madrid; Manila; Mumbai; Paris; Riyadh; Seoul; Tehran; Yangon). Yet in Lima, during March when lockdown was implemented, the core of the city brightened whilst the periphery dimmed. For some cities, hot spots of both dimming and brightening emerged (Bogota, Ho Chi Minh City; Hong Kong; Jakarta; Kinshasa Nairobi).

Where a whole city scale or spatially concentrated dimming of a city occurred, this is indicative of a variety of socio-spatial trends in response to COVID-19. Previous research on energy use and COVID-19 has evidenced substantial reductions in areas of concentrated economic activity[1] and a transfer of energy consumption into the domestic sphere. For example, Liu et al.[34] evidence increased activity in residential areas, decreased activities in commercial centres, and similar activity levels in transport and public facilities. In some cities a proportion of affluent or transient urban residents, no longer tied to places of employment, temporarily migrated away from dense urban areas where the perceived risks of contracting the virus are most acute[7], thus contributing towards a suburbanisation of energy consumption. In Wuhan where the virus first emerged, an estimated five million residents left the city prior to lockdown[35].

Further detailed analysis of cities with a spatially concentrated change offers insight into how NTL intensity is shaped by the degree and type of industrialisation in a city. Many highly industrialised areas - including energy intensive industrial zones and infrastructural corridors e.g. the Wuhan subsidiary of the China Baowu Steel Corporation, one of the foremost global steel producers. Dimming of major energy infrastructures is also apparent, reflecting the role of global energy systems and markets in shaping urban energy intensity. Riyadh Oil Refinery part of Saudi Aramco - a company with the world's second-largest proven crude oil reserves - dimmed as demand for oil hit a 25 year low in response to COVID-19[36].

Imagery also highlights cities that contradict trends of a reduction or suburbanisation of energy consumption. In Dar es Salaam (a city that brightened overall) restrictions on socio-economic activities were relatively light-touch attributed to the political response to the pandemic[37], coupled with concerns about impacts of lockdown on employment[38]. In selected cities, patterns also changed considerably over time. For example, in Lima one of the regions worst hit by COVID-19[39], a brightening of the core and dimming of the periphery from February until April gave way to a complete dimming in May and June.

Explaining changes in urban energy use through changes in mobility, stringency of government restrictions and COVID-19 incidence

The diversity of configurations evidenced over both space and time suggests that multiple factors shape changes in urban energy consumption in response to COVID-19. We examine the association between temporal shifts in energy use patterns, and changes in COVID-19 incidence and non-pharmaceutical measures. We recognise the distinctive dynamics of this association across cities by employing a hierarchical two-level modelling approach, at level 1 capturing time-city interactions and level 2 capturing city-specific patterns (see Methods Section). Monthly NTL imagery affords limited temporal granularity, so we used Google Mobility Report data to capture these dynamics. Changes in mobility, specifically in the share of stay-at-home population, serve as a proxy for shifts in urban energy use[40]. To measure non-pharmaceutical interventions, we used a stringency index which is a composite indicator that measures the extent and variation of non-pharmaceutical interventions globally, ranging from 0 (no measures) to 100 (the strictest scenario)[28].

We recognise two important features in the association between these factors. First, the relationship between changes in mobility (energy use), COVID-19 incidence and non-pharmaceutical measures represents multiple causal mechanisms, arising

from "top-down" government interventions and "bottom-up" individual responses. For instance, strict non-pharmaceutical measures may result in business and school closures, reducing mobility, increasing the share of stay-at-home population and ultimately domestic energy consumption. Conversely, rising COVID-19 case transmission, particularly early in the pandemic, may have led to increasing public concern fuelled by anxiety and fear with a rising number of stay-at-home population and domestic energy usage as a result of reduced workplace activity.

Second, these relationships exhibit different temporal dynamics across cities (Figure 6a and 6b). Certain cities (Melbourne, Kuala Lumpur, Delhi, Manila, Lagos) display large increases in stay-at-home population associated with strict non-pharmaceutical interventions despite relatively small rises in COVID-19 cases. Cities like Singapore, Paris, Madrid, Santiago and Lima show equally large increases in stay-at-home population and strict interventions; yet report consistently high numbers of COVID-19 cases. Others, including Bangkok and Seoul, display moderate increases in stay-at-home population despite strict non-pharmaceutical interventions.

Figure 6c-e reports our modelling of changes in the share of stay-at-home population as a function of stringency intervention and new COVID-19 cases (see Methods and SM Table 3 for full model estimates). Main fixed effects are displayed in Figure 6c, and random, varying city slopes for stringency and new COVID-19 cases in Figures 6d-6e, respectively. Compared to COVID-19 cases, a larger and positive estimate for local stringency measures ($\beta = 4.69; 95\%\ CI = 3.85 - 5.52$) (Figure 6c) suggests that the enactment of "top-down" stringent lockdown played a major role in incentivising working from home and hence domestic energy consumption across most cities in our sample. Coupled with a positive but smaller estimate for local stringency at time t-1 ($\beta = 2.73; 95\%\ CI = 2.02 - 3.45$), these findings also suggest that the largest impact of stringency measures on reducing travel-to-work activity was immediate but it takes some time for this to be fully realised.

Figure 6d-6e reveals the extent of variation in the association between changes in the share of stay-at-home population, and stringency measures and new COVID-19 cases across our sample of cities. Cross-tabulating estimates for these associations, we identify four groupings of cities (Figure 6f):

- Group one includes cities with greater than average stringency and COVID-19 cases estimates, (e.g. Kuala Lumpur, Manila and Mumbai). Underpinning these results are relatively high shares of stay-at-home population (40%) and arguably domestic energy use, coupled with high levels of stringency (100) and continuously small numbers of COVID-19 cases (<15 per million) (Figure 6a-b).

- Group two display larger than average stringency but lower COVID-19 cases estimates (e.g. Lagos, Bogota, Lima and Johannesburg). This reflects initially large and subsequently moderate increases in stay-at-home population (ranging from 40%-20%) and domestic energy use, and moderate rises in COVID-19 cases despite strict lockdown interventions early in the pandemic (i.e. March) (Figure 6a-b and SM Table 3).

- Group three includes cities with smaller than average stringency and COVID-19 case estimates (e.g. Bangkok, Osaka, Cairo, Moscow and New York). These cities display moderate rises in the share of stay-at-home population (<25%) and domestic energy use despite stringent measures, with varying outcomes of COVID-19 cases: persistently low in Bangkok, Osaka and Cairo, and relatively high in Moscow and New York.

- Group four comprises a small set of cities displaying small stringency but greater than average COVID-19 cases estimates (e.g. Seoul and Tokyo). These patterns reflect a trend of moderate stay-at-home population shares (<20%), low COVID-19 cases and stringency measures. In South Korea, transmission was controlled by employing less stringent social distancing measures than in Europe and the United States[41]. Similarly, Japan did not impose stringent lockdown measures, but enacted a state of emergency strategy to encourage people to stay at home[42].

These overarching trends suggest that "top-down" emergency restrictions and legislation introduced by national governments have played a substantial role in reconfiguring social and economic structures, and therefore energy consumption patterns, in the majority of cities selected. However, where government response has been relatively light touch, "bottom-up" changes in energy–related practices owing to the response of individuals or employers to the crisis assume greater importance in shaping energy consumption[43]. In the absence of emergency legislation, people are still required to engage in essential everyday activities that encourage energy consumption e.g. commuting. However, our results show that energy consumption and mobility declined moderately over time, as non-essential energy-related activities were foregone in response to the increased incidence of COVID-19.

Concluding remarks

Whilst global, and typically national, demand for energy fell overall in response to COVID-19 and accompanying restrictions (especially in contexts where per-capita energy use is typically high)[4] new spatial distributions have emerged between and

within cities. Our analysis of NTL intensity highlights the diversity of changes in energy consumption between and within cities, somewhat refuting dominant narratives of the "suburbanisation" of energy demand in many urban contexts. Further modelling with a range of contextual variables suggests that in most cities stringency of government's response to COVID-19 is likely a defining factor in shaping reductions in urban energy consumption.

There is ongoing debate about whether COVID-19 is likely to act as a catalyst for a permanent reduction in urban energy consumption owing to digitalisation of work and other activities[5], and indeed as inspiration for transitions to a low carbon society[44]. Our analysis supports the need for ambitious national and global policies that substantially reconfigure social and economic systems - rather than individual behaviour change - if the necessary scale of change for a low-carbon society is to be achieved.

There are a number of limitations to our analysis. Our analysis provides limited insight into energy-related household practices or industrial energy usage that do not emit light. For example, in Southern India increased domestic energy consumption for cooling emerged during COVID-19 as people were forced to stay at home during hot weather[45]. A focus on large urban conurbations means that we overlook the circulation of COVID-19 within smaller cities or rural and peri-urban areas, particularly during the later stages of the pandemic[22]. Finally, evidence of changes in energy consumption post-lockdown suggests that recovery to pre-lockdown levels is socially and spatially uneven, with relatively affluent areas experiencing a rapid recovery compared to poorer regions[9,11]. Detailed spatial analyses of NTL imagery beyond June 2020 could provide insight into the longer-term impacts of COVID-19, including inequalities embedded in the recovery of energy consumption levels post-lockdown.

Methods

Our analytical framework consists of four main stages. Each of these stages is in turn described below.

Night-time light (NTL) imagery. We used NTL satellite imagery to sense changes in urban energy consumption patterns. NTL imagery captures daily and detailed nocturnal visible light observations of the Earth, providing a unique source to monitor the spatial distribution and intensity variations of human activity at local and planetary scales in near-real time. NTL data have extensively been used to study electricity consumption, socio-economic activities, light pollution, urban extent changes and power outages[46].

We used a monthly composite of NTL data produced by the Payne Institute for Public Policy under the Colorado School of Mines (https://payneinstitute.mines.edu/eog/nighttime-lights/). We utilised the version 1 monthly series of global average radiance composite images from the Visible Infrared Imaging Radiometer Suite (VIIRS) Day-Night Band (DNB) sensor on the Suomi National Polar-orbiting Partnership satellite. The DNB encodes records of visible near-infrared NTL intensity which is measured in radiance units i.e. nanoWatts/cm2/sr ($nWcm^{-2}sr^{-1}$). The spatial resolution of VIIRS data is 15 arc-seconds ($450m$) across the latitudinal zone of $65^{\circ}S$-$75^{\circ}N5$, providing global coverage with 12hr revisit time[47]. The data version used in our study is the monthly VIIRS Cloud Mask product. These data are corrected for stray light as well as the effects of biogeophysical processes, such as seasonal vegetation and snow[48]. The data are however not corrected for temporal lights, including fires and boats. Following Li et al.[49], we used an empirical threshold of 0.3 $nWcm^{-2}sr^{-1}$ to remove dim light noises caused by these forms of temporal lights. The threshold was subtracted from the VIIRS image and negative pixel values were set to zero. This noise removal operation was conducted using Google Earth Engine. For our analysis, we used cloud free data, and assessed if zero values in the average radiance imagery for our sample of cities effectively encoded no lights, as regions towards the poles during summer months have no data due to solar illumination. As a result, imagery for six time points was excluded from the analysis (SM Figure 1).

Measuring city-scale changes. To measure the overall extent of changes in energy consumption patterns in cities, we computed three summary indicators. All three indicators are based on the difference between the radiance for individual months and for December (our baseline). The first indicator is the mean number of pixels (Equation 1). It indicates the number of pixels defining individual cities that recorded a change on average across pixel differences for individual months (m_t) and the baseline month (m_0) (i.e. December, 2019). Averages were computed conditionally for pixels indicating negative, neutral and positive change (C). The second indicator is the average percentage of pixels in each category: negative, neutral and positive (Equation 2). This indicator accounts for variations in city size to enable comparisons across cities. The third indicator is the median radiance (r) of night-time intensity across the six month differences. This indicator provides an approximate estimate of the strength of change in NTL intensity. For this indicator we only reported two categories; that is, positive and negative, as the median for the neutral category is zero. In addition to these indicators, we analysed the full distribution of the difference in NTL radiance between individual months and December, 2019. Given small numbers, extreme NTL scores (i.e. above 30) are set to 30.

$$n = \frac{\sum_{t=1,m\in C}^{6} m_t(C) - m_0(C)}{6} \tag{1}$$

$$p = \frac{\sum_{t=1,m\in C}^{6} \frac{m_t(C)-m_0(C)}{m_t-m_0}}{6} \tag{2}$$

$$n = \frac{\sum_{t=1,m\in C}^{6} median[r_t(C)-r_0(C)]}{6} \tag{3}$$

To define city extents, we used a set of Functional Urban Area (FUA) boundaries[25] developed in a collaborative project between the Organisation for Economic Co-operation and Development and the Global Human Settlement layer project. Delimiting the extent of cities is challenging, and the FUA boundaries overcome this problem providing a consistent way to define these extents based on population density measured at a fine spatial resolution ($1km^2$ grids). First, adjacent grids of high density are clustered together. Then the level of commuting flows is measured to integrate non-continuous areas but that display a distinctive urban centre of employment.

Analysing intra-urban changes. To understand intra-urban changes, we conducted two sets of analyses. First, we examined the association between population density and NTL intensity using Generalised Additive Models (GAMs). We sought to assess if more densely populated areas in cities experienced larger average declines in NTL intensity, arguably reflecting the location of employment centres. To this end, population density data were obtained from the WorldPop project (https://www.worldpop.org). These data comprise a raster layer covering the entire world and provide population density estimates at $1km^2$ grids. The data set is based on the United Nations' population count data using a top-down methodological approach[29]. In this approach, population counts at administrative units level are disaggregated to grid-cell based counts by using a series of detailed geospatial data sets, such as land cover, night-time imagery and proximity to amenities as covariates in a random forest estimation framework.

In a second analysis, we assessed the spatial distribution of NTL change between January and June, 2020. We mapped the changes in NTL intensity for individual cities, and classified them based on the spatial structure of these changes during the month local lockdowns were enacted or the following month if lockdowns were introduced towards the end of a month (SM Table 2 provides a list of start dates of local lockdowns for each city). We categorised cities into three classes: whole city, fragmented and spatially concentrated patterns of change. Whole city change encompasses cities displaying widespread dimmed or brightened patterns of NTL intensity. Fragmented change includes cities displaying scattered patterns of change. Spatially concentrated involves cities displaying spatially focused patterns of change. We observed three distinctive patterns: (1) changes along network infrastructures; (2) a core-periphery configuration; and, (3) systematic localised changes in key areas of cities.

Modelling mobility, stringency and COVID-19 infection. We also sought to understand the temporal patterns of urban energy use, non-pharmaceutical interventions and COVID-19 incidence. We used a hierarchical two-level modelling approach to capture time-city level interactions at level 1 and city-specific patterns at level 2. Monthly NTL data afford very limited temporal granularity, so we used Google Mobility Report data to capture these dynamics. We used the percentage change in stay-at-home population as a proxy for shifts in urban energy use. We argue that this is a reasonable proxy as we expect that increases in stay-at-home population and simultaneous drops in time spent at work over time would lead to be associated with changes in the patterns of urban energy use. Analysis of Google workplace and residential mobility data reveals that increases in stay-at-home population mirror declines in time spent at work (SM Figure 4).

We estimated a series of hierarchical regression models using the percentage change of stay-at-home population as a function of a stringency indicator and COVID-19 incidence in a generalised linear mixed model (GLMM) framework. Intuitively, all estimated models included a stringency indicator and COVID-19 incidence measured at time t, and a stringency indicator at time $t-1$ recognising the delayed effects of lockdowns on influencing mobility patterns. For interpretation and identification purposes, independent variables were standardised, subtracting the mean and dividing by the standard deviation. We used natural splines to account for systematic temporal variations in the data, and incorporated natural splines as overall and city-specific parameters. We also included a temporal autoregressive term to account for temporal dependency. We evaluated the inclusion of temporal lags of higher order for the stringency indicator and COVID-19 incidence. Correlation coefficients and estimates for these variables are very small in size and statistical significance. We report a correlation matrix and two models in the SM Table 3 and Figure 5 providing evidence for this.

More formally, we present evidence from three different model specifications in the manuscript (Figure 5). These models are mathematically formulated in Equations 4-6: y_{it} captures change in stay-at-home population at city i in time t; β_{0i} is the random intercept that varies across cities; β_{1i} is the slope of the associated stringency indicator s_{it}; β_{2i} is the slope of the lagged stringency indicator at $t-1$; β_{3i} is the slope of new COVID-19 cases c_{it}; $\sum_{k=1}^{n+1} \beta_{ki} B_{kit}$ represents random natural spline slopes at three knot points that vary across cities and capture systematic temporal patterns in stay-at-home population changes (see Hastie

et al.[50] for details on splines); ε_{it} is the city-time-level residual term that is assumed to be of first-order autoregressive (Ω_ε); that is, residuals are assumed to be correlated. Residuals at time $t-1$ are assumed to influence residuals at time t. Equations relating to β_{0i} and β_{ki} correspond to the random effects, or city-varying intercept and natural spline slopes, respectively. They capture variations in the associated parameters across cities and have unexplained heterogeneity denoted by u_{0i} and u_{ki}. These error terms follow an independent normal distribution $N(0,\sigma^2_{u0})$ and $N(0,\sigma^2_{u1})$.

$$
\begin{aligned}
y_{it} &= \beta_{0i} + \beta_{1i}s_{it} + \beta_{2i}s_{it-1} + \beta_{3i}c_{it} + \sum_{k=1}^{n+1}\beta_{ki}B_{kit} + \varepsilon_{it} \\
\beta_{0i} &= \beta_0 + u_{0i} \\
\beta_{ki} &= \beta_k + u_{ki} \\
\varepsilon_{it} &\sim N(0,\Omega_\varepsilon)
\end{aligned}
\tag{4}
$$

The key difference across Equations 4-6 is in the parameter allowed to vary across cities. In Equation 4, natural spline parameters are allowed to vary across cities capturing differences of systematic temporal fluctuations in stay-at-home population. We report the estimates for β_{1i}, β_{2i} and β_{3i} from this model as it provides the smallest Akaike Information Criterion (*AIC*) score. Though coefficients across all three models are fairly consistent in size. In Equation 5, β_{1i} is allowed to vary across cities. This coefficient captures differences in the association between changes in stay-at-home population and the stringency indicator. In Equation 6, β_{3i} is allowed to vary across cities. This coefficient captures differences in the association between changes in stay-at-home population and new COVID-19 cases. In addition, Equation 6 also includes a lagged term (β_{4i}) for new COVID-19 cases to capture one period delay in the relationship between changes in stay-at-home population and new COVID-19 cases. All models included natural spline parameters in the fixed part of the model and a first-order autoregressive error term was assumed for the city-time level residuals.

$$
\begin{aligned}
y_{it} &= \beta_{0i} + \beta_{1i}s_{it} + \beta_{2i}s_{it-1} + \beta_{3i}c_{it} + \sum_{k=1}^{n+1}\beta_{ki}B_{kit} + \varepsilon_{it} \\
\beta_{0i} &= \beta_0 + u_{0i} \\
\beta_{1i} &= \beta_1 + u_{1i} \\
\varepsilon_{it} &\sim N(0,\Omega_\varepsilon)
\end{aligned}
\tag{5}
$$

$$
\begin{aligned}
y_{it} &= \beta_{0i} + \beta_{1i}s_{it} + \beta_{2i}s_{it-1} + \beta_{3i}c_{it} + \beta_{4i}c_{it-1} + \sum_{k=1}^{n+1}\beta_{ki}B_{kit} + \varepsilon_{it} \\
\beta_{0i} &= \beta_0 + u_{0i} \\
\beta_{3i} &= \beta_3 + u_{3i} \\
\varepsilon_{it} &\sim N(0,\Omega_\varepsilon)
\end{aligned}
\tag{6}
$$

Google Mobility Data: In response to COVID-19, Google released Community Mobility Reports to help inform public health responses to COVID-19 (https://www.google.com/covid19/mobility/). The data set measures the change in the number of visitors (or time spent) in relation to a baseline period. The baseline corresponds to the median value from the 5–week period Jan 3-Feb 6, 2020. The changes are categorised according to specific places or sectors: retail and recreation; groceries and pharmacies; parks; transit stations; workplaces; and residential. We focused our analysis on the residential category which indicates the change in stay-at-home population.

Stringency index: we used a stringency index to capture the level and variation of non-pharmaceutical interventions (https://covidtracker.bsg.ox.ac.uk). It is a composite indicator based on nine response indicators: school closures; workplace closures; cancellation of public events; restrictions on gatherings; public transport restrictions; public information campaigns; and stay at home measures[28]. The index, available since 1st January 2020, computes a simple score by adding together the nine indicators which is rescaled to vary between 0 and 100. The stringency index is intended for comparative purposes, rather than as an indicator of how effective national policies have been at tackling the spread of COVID-19[28].

COVID-19 cases: Data on the new number of COVID-19 cases were obtained from Our World in Data[30]. We also analysed the relationship between COVID-19 deaths and changes in stay-at-home population. We do not report these analyses in the main manuscript as we argue that COVID-19 cases were a more prominent measure of public knowledge in the early stages of the pandemic. We believe that individual responses during this period were more a result of the extent and rate of spread of COVID-19, rather than the actual number of deaths. We do however report analysis on COVID-19 in the SM Figure 3 and 4.

Data availability

The data used for our analysis is publicly available online: monthly VIIRS NTL satellite imagery composites (version 1) from the Earth Observations Group (EOG) Payne Institute for Public Policy, https://eogdata.mines.edu/download_dnb_composites.html; daily COVID-19 pandemic data from Our World in Data, https://github.com/owid/covid-19-data/tree/master/public/data; social distancing and lockdown data from the Oxford Covid-19 Government Response Tracker (OxCGRT), https://github.com/OxCGRT/covid-policy-tracker; Google mobility data, https://www.google.com/covid19/mobility/; and, global population data from the WorldPop project, https://www.worldpop.org/project/categories?id=18. The results supporting the findings of this study are provided in the main text and Supplementary Information. The source data underlying all the figures in the main manuscript and Supplementary Information are provided as a Source Data file. Source data to replicate the results reported in the paper are provided in an Open Science Framework (OSF) repository, DOI: [xxx] (https://xxx), except for the monthly VIIRS NTL imagery composites which exceed the data storage capacity in Github. VIIRS NTL composites can be obtained from the first link provided in this paragraph.

Code availability

The code to reproduce all the analysis and figures reported in this study are openly available on an Open Science Framework (OSF) repository, DOI: [xxx] (https://xxx). The analysis was performed in RStudio 1.3.959 running on R version 4.0.2 (2020-06-22) using the following list of packages sorted in alphabetical order: "countrycode 1.2.0", "corrplot 0.84", "glmmTMB 1.0.2.1", "ggpubr 0.4.0", "grid 4.0.2", "gridExtra 2.3", "lubridate 1.7.9", "osmdata 0.1.3", "raster 3.3-13", "rvest 0.3.6", "sf 0.9-5", "tmaptools 3.1", "tidyverse 1.3.0", "viridis 0.5.1". Refer to the README in the repository for instructions.

References

1. Ruan, G. *et al.* A cross-domain approach to analyzing the short-run impact of covid-19 on the us electricity sector. *Joule* **4**, DOI: 10.1016/j.joule.2020.08.017 (2020).
2. Agency, I. E. The covid-19 crisis is causing the biggest fall in global energy investment in history. Tech. Rep. (2020).
3. Fund, I. M. World economic outlook update, april 2021. Tech. Rep. (2021).
4. Agency, I. E. Global energy review 2021. Tech. Rep. (2021).
5. Kanda, W. & Kivimaa, P. What opportunities could the covid-19 outbreak offer for sustainability transitions research on electricity and mobility? *Energy Res. & Soc. Sci.* **68**, DOI: 10.1016/j.erss.2020.101666 (2020).
6. Geels, F. W., Sovacool, B. K., Schwanen, T. & Sorrell, S. The socio-technical dynamics of low-carbon transitions. *Joule* **1**, DOI: 10.1016/j.joule.2017.09.018 (2017).
7. Connolly, C., Ali, S. H. & Keil, R. On the relationships between covid-19 and extended urbanization. *Dialogues Hum. Geogr.* **10**, DOI: 10.1177/2043820620934209 (2020).
8. Batty, M. The coronavirus crisis: What will the post-pandemic city look like? *Environ. Plan. B: Urban Anal. City Sci.* **47**, DOI: 10.1177/2399808320926912 (2020).
9. Zheng, B. *et al.* Satellite-based estimates of decline and rebound in china's co ₂ emissions during covid-19 pandemic. *Sci. Adv.* **6**, DOI: 10.1126/sciadv.abd4998 (2020).
10. Graff, M. & Carley, S. Covid-19 assistance needs to target energy insecurity. *Nat. Energy* **5**, DOI: 10.1038/s41560-020-0620-y (2020).
11. Aruga, K., Islam, M. M. & Jannat, A. Effects of covid-19 on indian energy consumption. *Sustainability* **12**, DOI: 10.3390/su12145616 (2020).
12. Beyer, R. C., Franco-Bedoya, S. & Galdo, V. Examining the economic impact of covid-19 in india through daily electricity consumption and nighttime light intensity. *World Dev.* **140**, DOI: 10.1016/j.worlddev.2020.105287 (2021).
13. Kuzemko, C. *et al.* Covid-19 and the politics of sustainable energy transitions. *Energy Res. & Soc. Sci.* **68**, DOI: 10.1016/j.erss.2020.101685 (2020).
14. fei Chen, C., de Rubens, G. Z., Xu, X. & Li, J. Coronavirus comes home? energy use, home energy management, and the social-psychological factors of covid-19. *Energy Res. & Soc. Sci.* **68**, DOI: 10.1016/j.erss.2020.101688 (2020).
15. Norouzi, N., de Rubens, G. Z., Choupanpiesheh, S. & Enevoldsen, P. When pandemics impact economies and climate change: Exploring the impacts of covid-19 on oil and electricity demand in china. *Energy Res. & Soc. Sci.* **68**, DOI: 10.1016/j.erss.2020.101654 (2020).

16. Gebreslassie, M. G. Covid-19 and energy access: An opportunity or a challenge for the african continent? *Energy Res. & Soc. Sci.* **68**, DOI: 10.1016/j.erss.2020.101677 (2020).

17. Memmott, T., Carley, S., Graff, M. & Konisky, D. M. Sociodemographic disparities in energy insecurity among low-income households before and during the covid-19 pandemic. *Nat. Energy* **6**, DOI: 10.1038/s41560-020-00763-9 (2021).

18. Broto, V. C. & Kirshner, J. Energy access is needed to maintain health during pandemics. *Nat. Energy* **5**, DOI: 10.1038/s41560-020-0625-6 (2020).

19. Brosemer, K. *et al.* The energy crises revealed by covid: Intersections of indigeneity, inequity, and health. *Energy Res. & Soc. Sci.* **68**, DOI: 10.1016/j.erss.2020.101661 (2020).

20. Bahmanyar, A., Estebsari, A. & Ernst, D. The impact of different covid-19 containment measures on electricity consumption in europe. *Energy Res. & Soc. Sci.* **68**, DOI: 10.1016/j.erss.2020.101683 (2020).

21. Gillingham, K. T., Knittel, C. R., Li, J., Ovaere, M. & Reguant, M. The short-run and long-run effects of covid-19 on energy and the environment. *Joule* **4**, DOI: 10.1016/j.joule.2020.06.010 (2020).

22. Acuto, M. *et al.* Seeing covid-19 through an urban lens. *Nat. Sustain.* **3**, DOI: 10.1038/s41893-020-00620-3 (2020).

23. Bustamante-Calabria, M. *et al.* Effects of the covid-19 lockdown on urban light emissions: Ground and satellite comparison. *Remote. Sens.* **13**, DOI: 10.3390/rs13020258 (2021).

24. United Nations. Work urbanization prospects 2018: Highlights. Tech. Rep., United Nations (2018).

25. Schiavina, M., Moreno-Monroy, A., Maffenini, L. & Veneri, P. Ghsl-oecd functional urban areas. Tech. Rep., Publications Office of the European Union, (2019).

26. Filho, C. R. D. S., Jr, J. Z. & Elvidge, C. Brazil's 2001 energy crisis monitored from space. *Int. J. Remote. Sens.* **25**, DOI: 10.1080/01431160410001662220 (2004).

27. Xu, G., Xiu, T., Li, X., Liang, X. & Jiao, L. Lockdown induced night-time light dynamics during the covid-19 epidemic in global megacities. *Int. J. Appl. Earth Obs. Geoinformation* **102**, DOI: 10.1016/j.jag.2021.102421 (2021).

28. Hale, T. *et al.* A global panel database of pandemic policies (oxford covid-19 government response tracker). *Nat. Hum. Behav.* **5**, DOI: 10.1038/s41562-021-01079-8 (2021).

29. Stevens, F. R., Gaughan, A. E., Linard, C. & Tatem, A. J. Disaggregating census data for population mapping using random forests with remotely-sensed and ancillary data. *PLOS ONE* **10**, DOI: 10.1371/journal.pone.0107042 (2015).

30. Ritchie, H. *et al.* Coronavirus pandemic (covid-19). *Our World Data* (2020). Https://ourworldindata.org/coronavirus.

31. Google. Google covid-19 community mobility reports. Available at https://www.google.com/covid19/mobility/ (01/07/2021).

32. Phillips, N. The coronavirus is here to stay — here's what that means. *Nature* **590**, DOI: 10.1038/d41586-021-00396-2 (2021).

33. Hamidi, S., Sabouri, S. & Ewing, R. Does density aggravate the covid-19 pandemic? *J. Am. Plan. Assoc.* **86**, DOI: 10.1080/01944363.2020.1777891 (2020).

34. Liu, Q. *et al.* Spatiotemporal patterns of covid-19 impact on human activities and environment in mainland china using nighttime light and air quality data. *Remote. Sens.* **12**, DOI: 10.3390/rs12101576 (2020).

35. Pinghui, J. & Ma, Z. 5 million left wuhan before lockdown, 1,000 new coronavirus cases expected in city (2020).

36. Ambrose, J. Oil prices slump as markets face lowest demand in 25 years. (2020).

37. Makoni, M. Tanzania refuses covid-19 vaccines. *The Lancet* **397**, DOI: 10.1016/S0140-6736(21)00362-7 (2021).

38. Mfinanga, S. G. *et al.* Tanzania's position on the covid-19 pandemic. *The Lancet* **397**, DOI: 10.1016/S0140-6736(21)00678-4 (2021).

39. Munayco, C. V. *et al.* Early transmission dynamics of covid-19 in a southern hemisphere setting: Lima-peru: February 29th–march 30th, 2020. *Infect. Dis. Model.* **5**, 338–345 (2020).

40. Mohammadi, N. & Taylor, J. E. Urban energy flux: Spatiotemporal fluctuations of building energy consumption and human mobility-driven prediction. *Appl. Energy* **195**, DOI: 10.1016/j.apenergy.2017.03.044 (2017).

41. Watanabe, T. & Yabu, T. Japan's voluntary lockdown. *PLOS ONE* **16**, DOI: 10.1371/journal.pone.0252468 (2021).

42. Dighe, A. *et al.* Response to covid-19 in south korea and implications for lifting stringent interventions. *BMC Medicine* **18**, DOI: 10.1186/s12916-020-01791-8 (2020).

43. Schot, J., Kanger, L. & Verbong, G. The roles of users in shaping transitions to new energy systems. *Nat. Energy* **1**, DOI: 10.1038/nenergy.2016.54 (2016).

44. Henry, M. S., Bazilian, M. D. & Markuson, C. Just transitions: Histories and futures in a post-covid world. *Energy Res. & Soc. Sci.* **68**, DOI: 10.1016/j.erss.2020.101668 (2020).

45. Singh, S. Covid-19 lockdown impact: Power demand drops as offices stay plugged out (2020).

46. Levin, N. *et al.* Remote sensing of night lights: A review and an outlook for the future. *Remote. Sens. Environ.* **237**, DOI: 10.1016/j.rse.2019.111443 (2020).

47. Cao, C. *et al.* Noaa technical report nesdis 142 visible infrared imaging radiometer suite (viirs) sensor data record (sdr) user's guide version 1.3. *NOAA Tech. Rep. NESDIS 142* 1–40 (2017).

48. Miller, S. *et al.* Illuminating the capabilities of the suomi national polar-orbiting partnership (npp) visible infrared imaging radiometer suite (viirs) day/night band. *Remote. Sens.* **5**, DOI: 10.3390/rs5126717 (2013).

49. Li, X., Zhou, Y., Zhao, M. & Zhao, X. A harmonized global nighttime light dataset 1992–2018. *Sci. Data* **7**, DOI: 10.1038/s41597-020-0510-y (2020).

50. Hastie, T., Tibshirani, R. & Friedman, J. *The Elements of Statistical Learning* (Springer New York, 2009).

Acknowledgements

Author contributions statement

Competing interests

The authors declare no competing interests.

Additional information

Supplementary information is available for this paper and has been submitted with the manuscript.

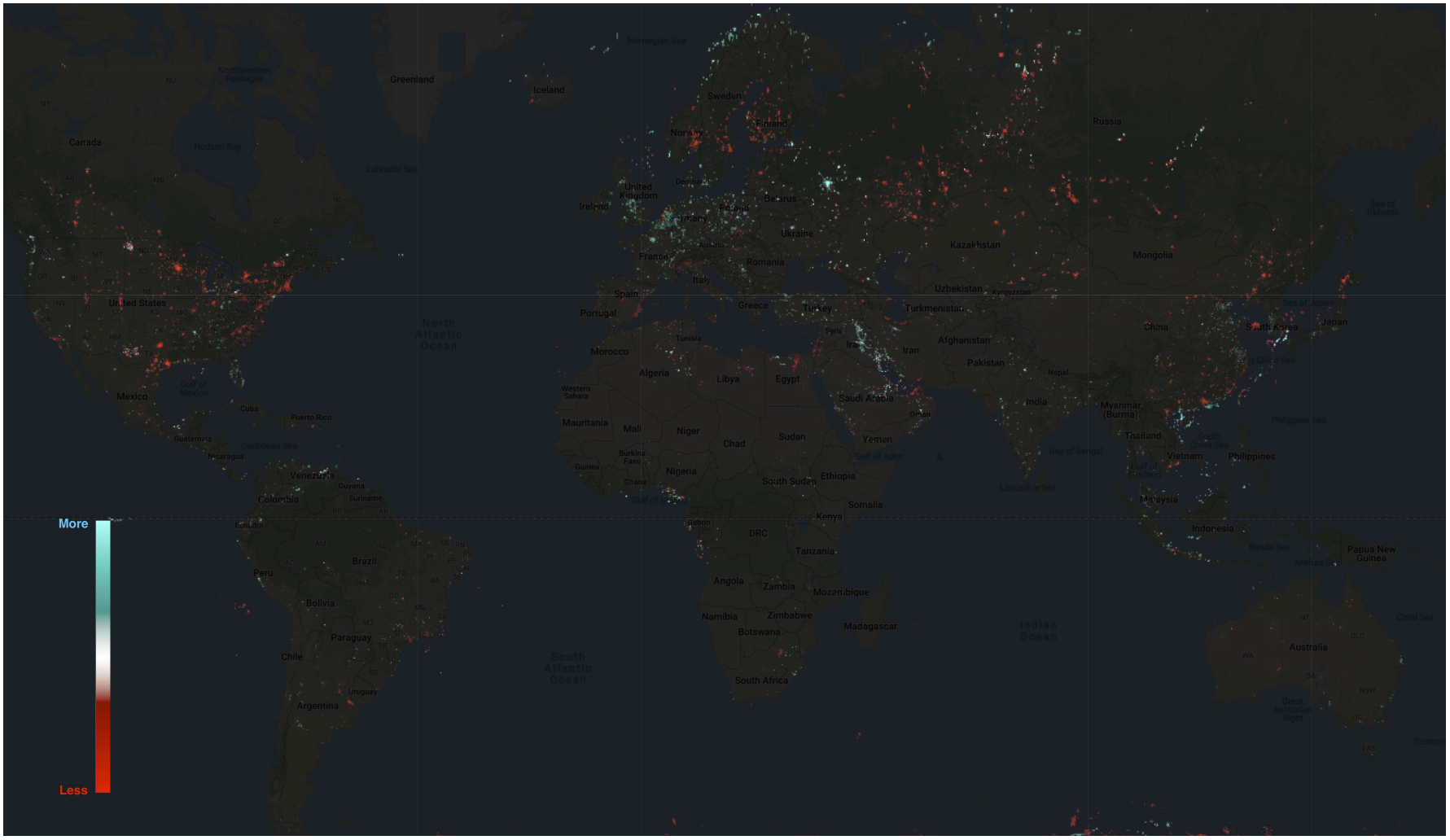

Figure 1. Global map of NTL intensity. Difference in radiance between December 2019 and March 2020. Red encodes a reduction in NTL intensity (i.e. dimmed). Blue encodes an increase (i.e. brightened). NTL imagery was extracted from the Payne Institute for Public Policy (https://payneinstitute.mines.edu/eog/nighttime-lights/).

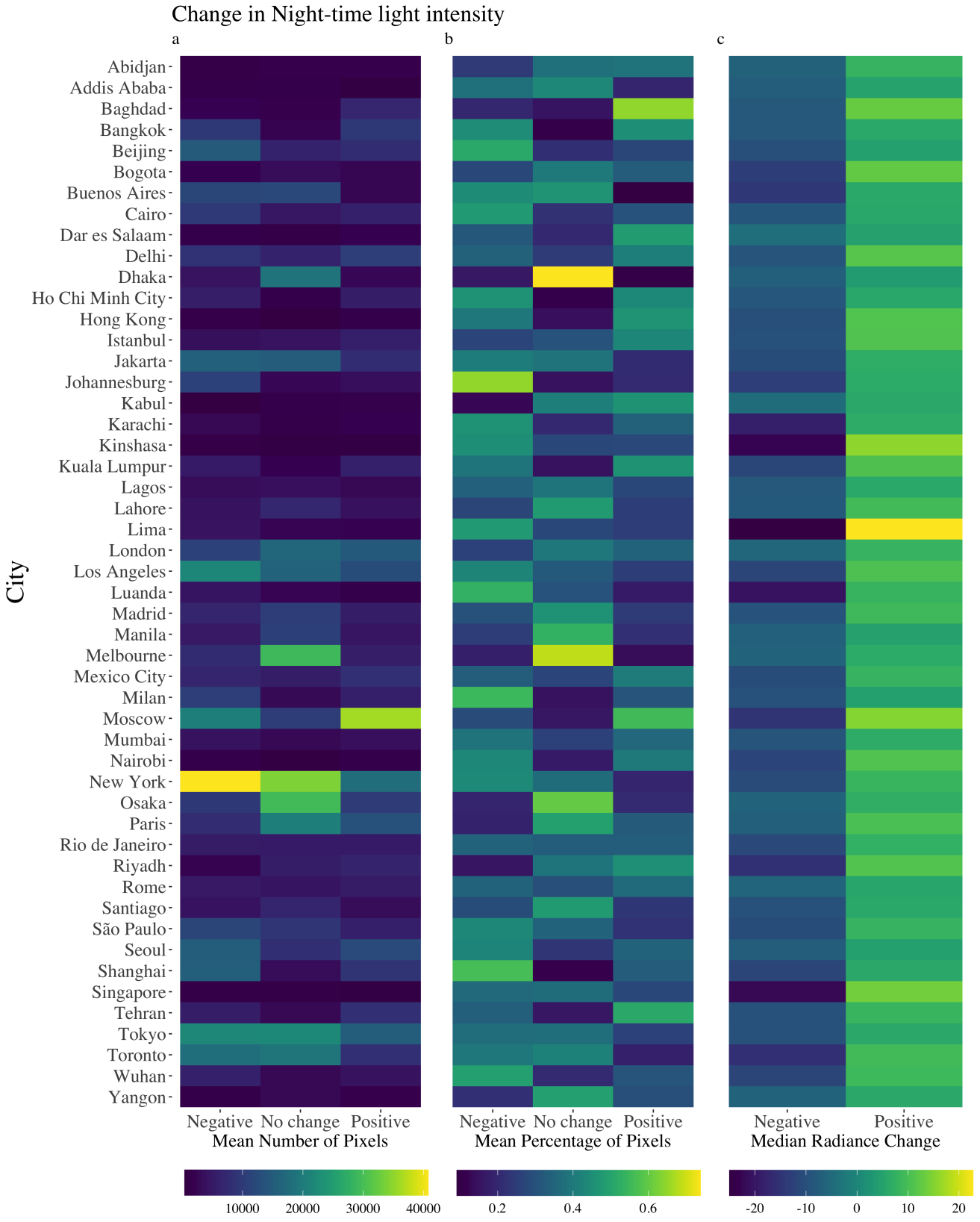

Figure 2. Indicators of changes in NTL intensity. **a** Mean number of pixels: Average number of changing pixels. **b** Mean percentage of pixels. **c** Median radiance change: Median radiance of NTL intensity. These indicators refer to the difference between individual months (January-June 2020) and December 2019 across three categories: negative, neutral and positive. NTL imagery was extracted from the Payne Institute for Public Policy (https://payneinstitute.mines.edu/eog/nighttime-lights/).

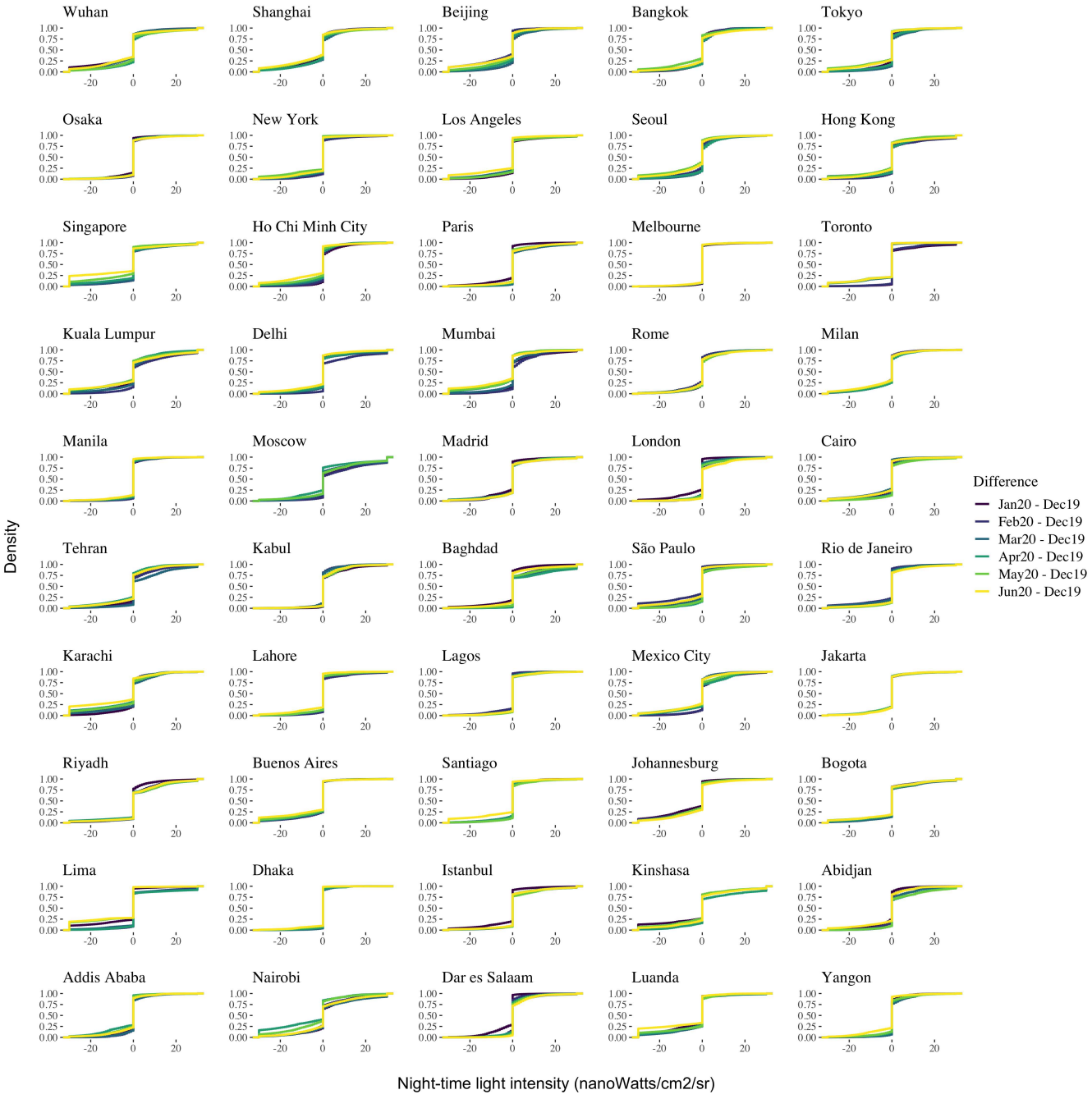

Figure 3. Change in NTL intensity. Each line represents the difference in NTL intensity between an individual months (January 2020 - June 2020) and December 2019 (baseline). NTL imagery was extracted from the Payne Institute for Public Policy (https://payneinstitute.mines.edu/eog/nighttime-lights/)

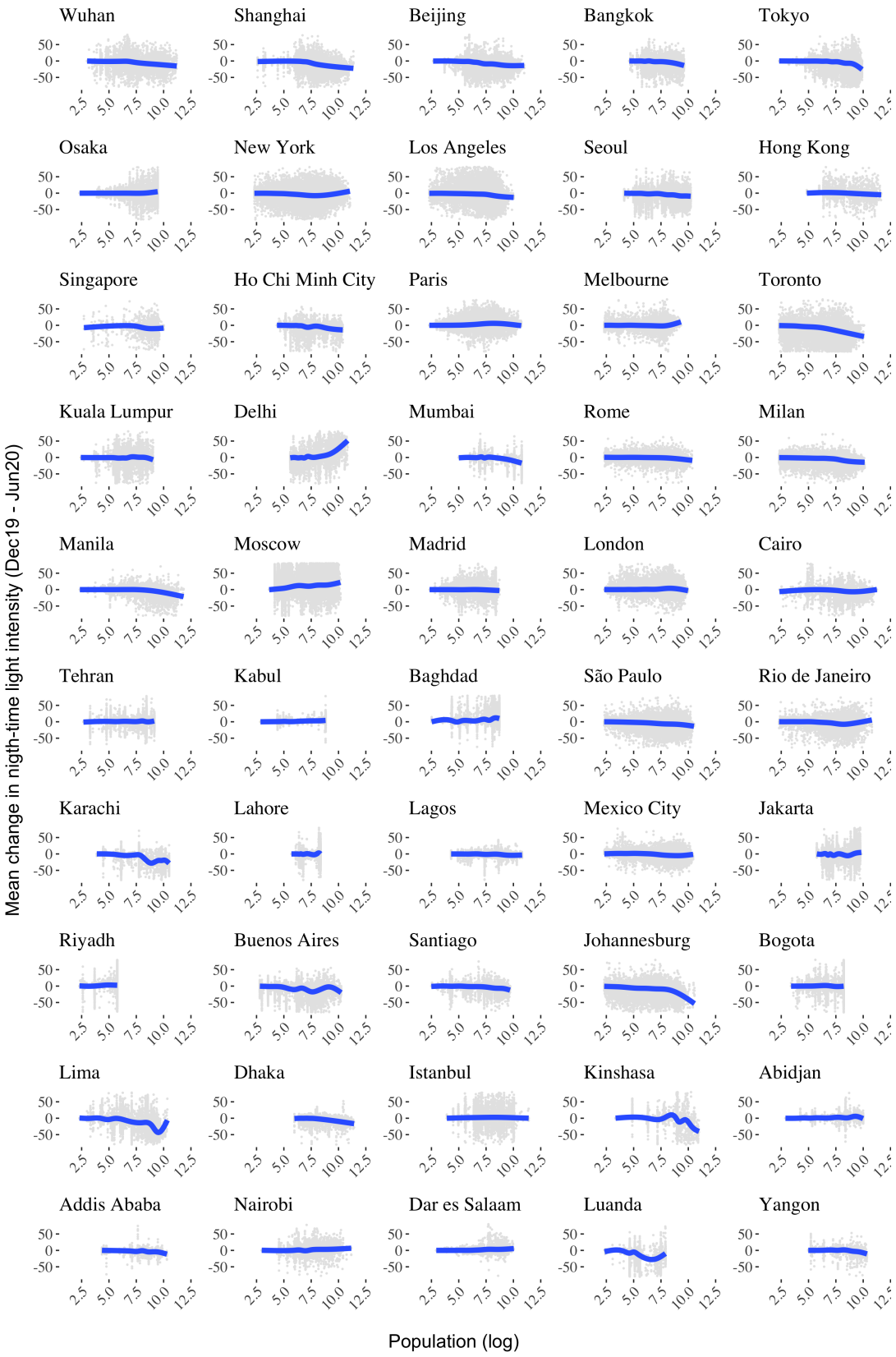

Figure 4. Relationship between population density (log) and average change in NTL intensity. The average in NTL intensity corresponds to the difference across individual months (January - June 2020) and December 2019 (baseline). NTL imagery was extracted from the Payne Institute for Public Policy (https://payneinstitute.mines.edu/eog/nighttime-lights/). Population density data were obtained from the WordPop project (https://www.worldpop.org - see Stevens et al., 2015).

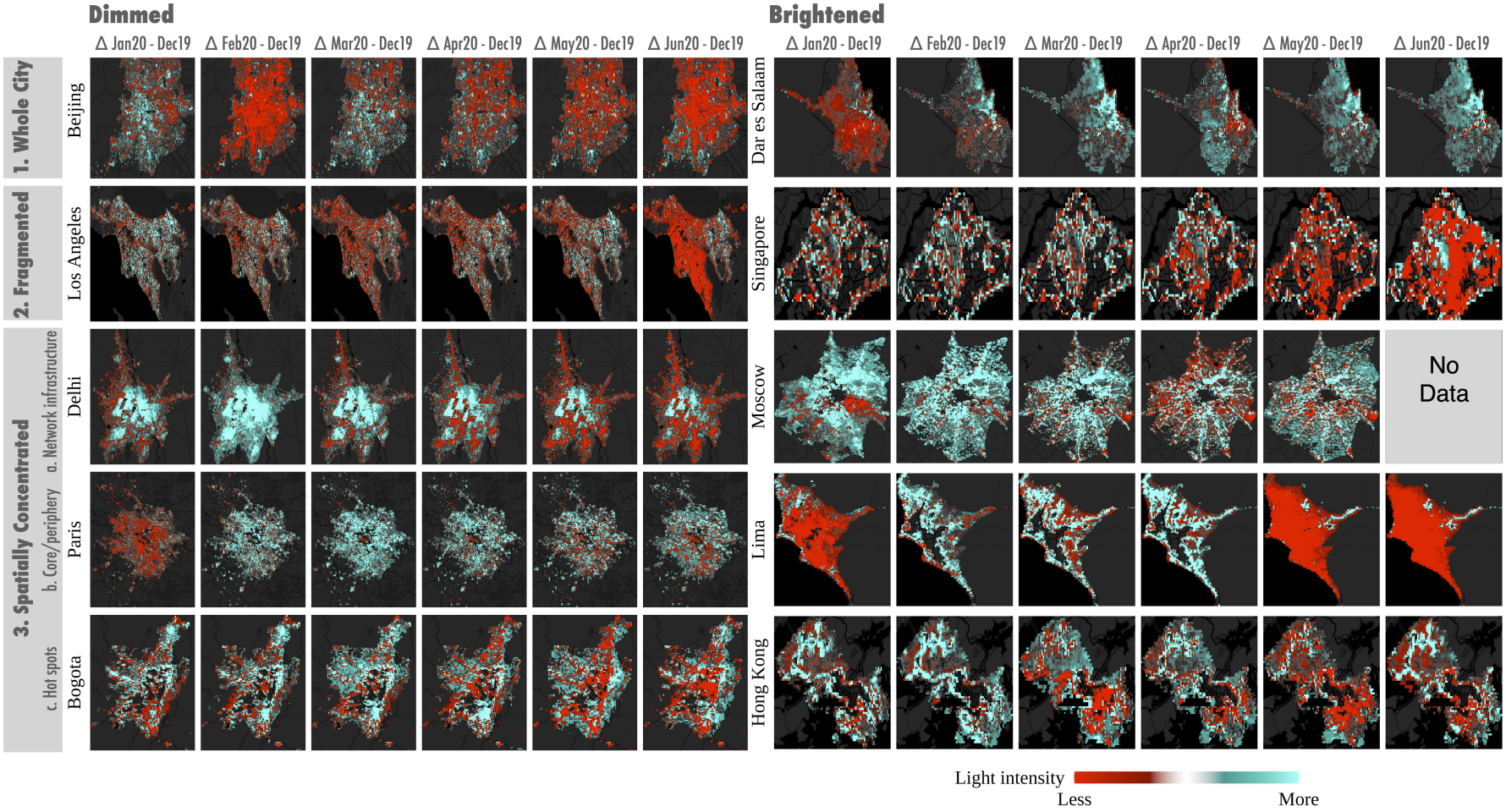

Figure 5. Classification of global cities according to change in NTL intensity. Pixels shaded in red record a reduction NTL intensity (i.e. dimmed), whilst those shaded in blue record an increase (i.e. brightened). Areas that did not experience a change are not shaded. Interpretation of the imagery in the text is based on the month that national lockdown was first imposed in each city (SM Table 2). Where the date of lockdown was close to the end of the month, imagery for the following month was used. NTL imagery was extracted from the Payne Institute for Public Policy (https://payneinstitute.mines.edu/eog/nighttime-lights/).

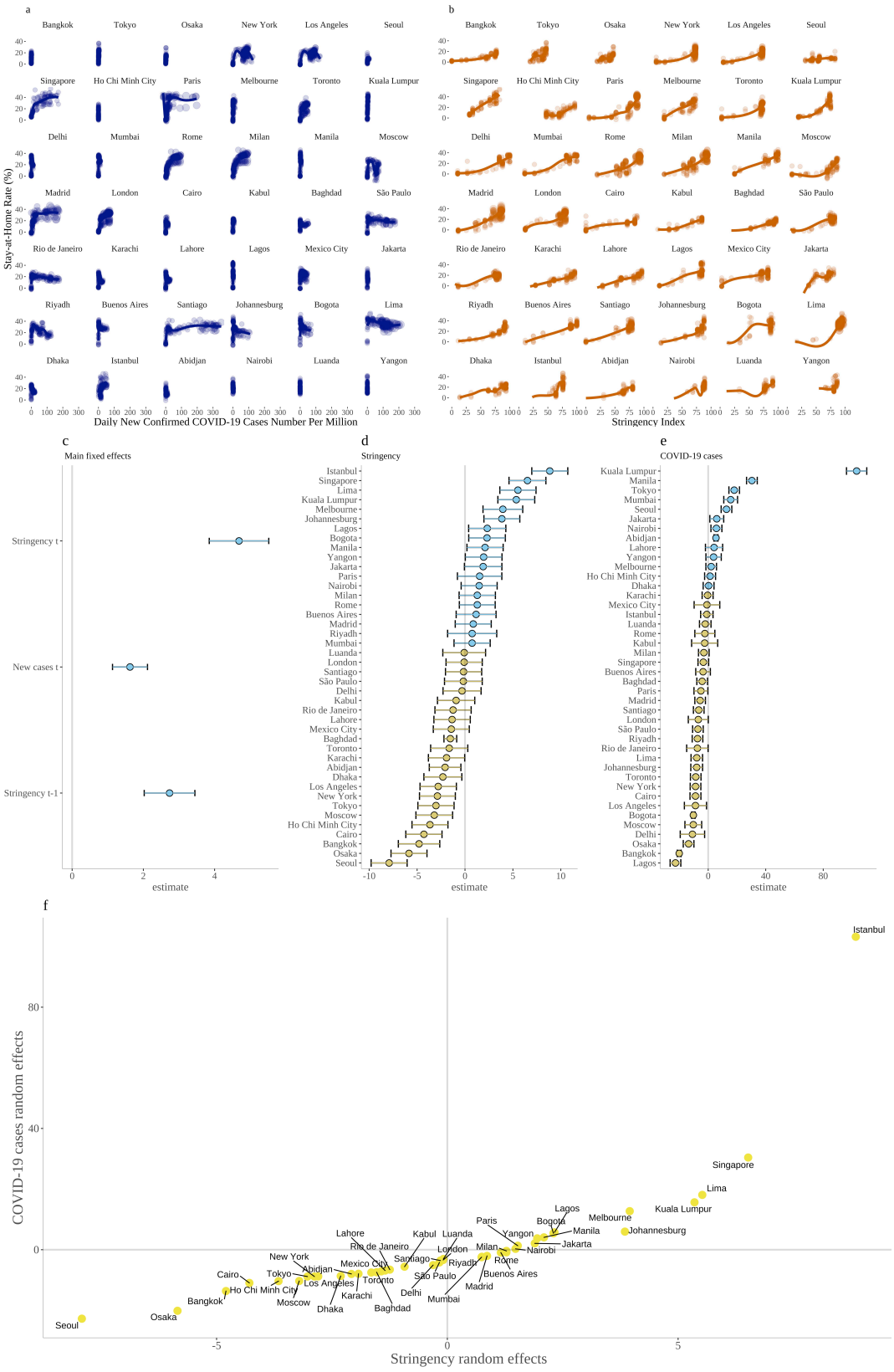

Figure 6. Association between stay-at-home population, stringency and COVID-19 cases. a Relationship between stay-at-home population and new COVID-19 cases per million. **b** Relationship between stay-at-home population and stringency index. **c** Regression coefficients: main fixed effects were obtained from Equation 4. **d** Regression coefficients: random effects for stringency across cities were obtained from Equation 5. **e** Regression coefficients: random effects for COVID-19 cases across cities were obtained from Equation 6. **f** Classification based on stringency and COVID-19 cases random effects estimated via Equation 5 and 6.

Supplementary Files

This is a list of supplementary files associated with this preprint. Click to download.

- nepapersm.pdf